Tricritical curve of massive chiral Gross-Neveu model with isospin

Michael Thies*

Institut für Theoretische Physik, Universität Erlangen-Nürnberg, D-91058 Erlangen, Germany

(Received 9 August 2022; accepted 15 September 2022; published 30 September 2022)

We reconsider the two-flavor version of the massive chiral Gross-Neveu model in $1+1$ dimensions. Its phase diagram as a function of baryon chemical potential, isospin chemical potential, and temperature has previously been explored. We recapitulate the results, adding the missing tricritical curves. They can be determined exactly by extending the standard stability analysis, using fourth-order almost degenerate perturbation theory. Results for three different bare masses are presented and discussed.

DOI: 10.1103/PhysRevD.106.056026

I. INTRODUCTION

The two best known Gross-Neveu (GN) models [1] are the original one with discrete chiral symmetry ($\psi \to \gamma_5\psi$) and Lagrangian

$$\mathcal{L}_{\rm GN} = \bar\psi i\partial\!\!\!/\psi + \frac{g^2}{2}(\bar\psi\psi)^2 \tag{1}$$

and the chiral GN model with U(1) chiral symmetry ($\psi \to e^{i\gamma_5\alpha}\psi$),

$$\mathcal{L}_{\rm NJL} = \bar\psi i\partial\!\!\!/\psi + \frac{g^2}{2}[(\bar\psi\psi)^2 + (\bar\psi i\gamma_5\psi)^2]. \tag{2}$$

We will only be dealing with $1+1$ dimensions and the large N_c limit of fermions with a U(N_c) "color" symmetry. We refer to the fermions as quarks and to flavor as color, following the common practice used in the Nambu–Jona-Lasinio (NJL) model in $3+1$ dimensions. Color indices will be suppressed as usual ($\bar\psi\psi = \sum_{k=1}^{N_c}\bar\psi_k\psi_k$ etc.). Extending model (2) to SU(2) chiral symmetry by introducing isospin, we arrive at the Lagrangian

$$\mathcal{L}_{\rm isoNJL} = \bar\psi i\partial\!\!\!/\psi + \frac{G^2}{2}[(\bar\psi\psi)^2 + (\bar\psi i\gamma_5\vec\tau\psi)^2], \tag{3}$$

familiar from the standard NJL model in $3+1$ dimensions [2]. As already indicated in the subscripts of the Lagrangians, we shall refer to (1) as GN model, (2) as NJL model, and (3) as NJL model with isospin (isoNJL).

*michael.thies@gravity.fau.de

Actually, the focus of the present work will be on the massive versions of these models obtained by adding a Dirac mass term (bare mass m_b)

$$\delta\mathcal{L} = -m_b\bar\psi\psi. \tag{4}$$

However, by way of introduction, we find it appropriate to briefly recall what is known about the phase diagrams of models (1)–(3) in the chiral limit [3].

The starting point for solving the isoNJL model (3) in the large N_c limit is the Dirac Hartree-Fock (HF) equation,

$$(-i\gamma_5\partial_x + \gamma^0 S + i\gamma^1\vec\tau\cdot\vec P - \mu - \nu\tau_3)\psi = \omega\psi. \tag{5}$$

We have introduced a baryon chemical potential μ and an isospin chemical potential ν. The scalar and pseudoscalar mean fields $S, \vec P$ satisfy the following self-consistency conditions:

$$\begin{aligned} S &= -G^2\langle\bar\psi\psi\rangle, \\ \vec P &= -G^2\langle\bar\psi i\gamma_5\vec\tau\psi\rangle, \end{aligned} \tag{6}$$

where the brackets denote either ground state or thermal averages. Let us now assume that the charged pseudoscalar condensate vanishes, $\vec P_\perp = 0$. Then the HF Hamiltonian becomes diagonal in isospin space with

$$(-i\gamma_5\partial_x + \gamma^0 S \pm i\gamma^1 P_3 - \mu \mp \nu)\psi = \omega\psi, \tag{7}$$

for isospin up and down, respectively. In each isospin channel, the Dirac HF equation reduces to that of a single-flavor NJL model. For isospin up, the mean field is $\Delta = S - iP_3$ and the chemical potential $\mu+\nu$. For isospin down, the corresponding parameters are $\Delta = S + iP_3$ and $\mu-\nu$. Although the HF Hamiltonian is diagonal in isospin, the two isospin channels are still coupled through

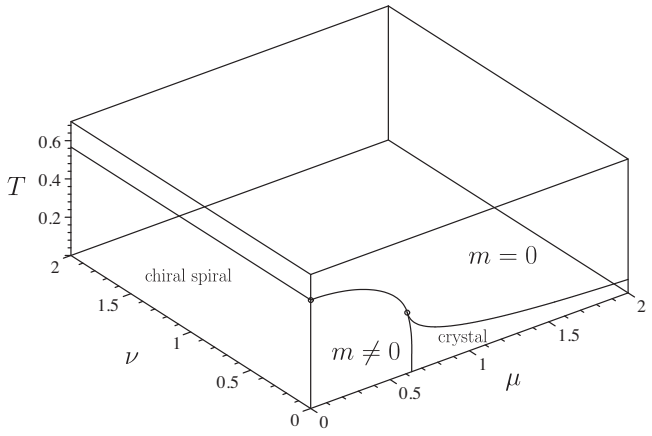

FIG. 1. Boundary phase diagram of the massless isoNJL model if one of the chemical potentials vanishes. At $\nu = 0$, it is the same as the massless GN model. At $\mu = 0$, it is the same as the massless NJL model with chemical potential ν.

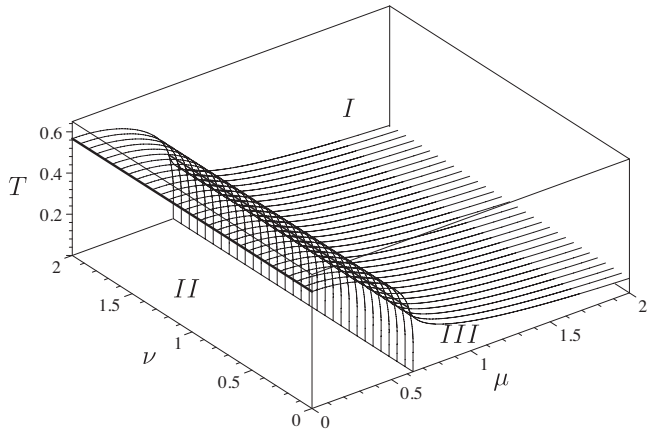

FIG. 2. Phase diagram of the massless isoNJL model in the bulk of (μ, ν, T) space. The phase boundary sheets result from moving the GN phase diagram rigidly into the direction of the ν axis. *I*) chirally restored phase, *II*) chiral spiral with constant radius, *III*) chiral spiral with radius modulated by GN soliton crystal.

the self-consistency condition, as P_3 involves the difference between up and down contributions.

It is now easy to see that the phase diagram of the isoNJL model in (μ, ν, T) space can be constructed from the known phase diagrams of the GN and NJL models in (μ, T) space. To this end, consider first the special cases where one of the chemical potentials vanishes. For $\nu = 0$ (pure baryon chemical potential), the NJL equations for isospin up and down have the same chemical potential μ and complex conjugate mean fields $\Delta = S \mp iP_3$. This is only possible if Δ is real ($P_3 = 0$). Thus the isoNJL phase diagram in the $\nu = 0$ plane is identical to the GN phase diagram in the (μ, T) plane, as indeed first noticed in the numerical study [4]. The GN phase diagram, in turn, is known analytically [5] and features three phases, a chirally restored one, a homogeneous massive one, and a soliton crystal. For $\mu = 0$ on the other hand (pure isospin chemical potential ν), the NJL equations (5) have opposite chemical potentials $\pm\nu$, and the mean fields are complex conjugates. This is exactly what it takes to solve both equations with the standard NJL solution, so that the phase diagram of the isoNJL model in the $\mu = 0$ plane is that of the one-flavor NJL model with chemical potential ν. It is also well-known analytically and consists of a chirally restored phase and a soliton crystal of "chiral spiral" type [6,7]. Thus, the phase diagram of the isoNJL model on the boundaries $\nu = 0$, $\mu = 0$ is completely determined by the single-flavor GN and NJL phase diagrams, see Fig. 1.

How can these boundary phase diagrams be continued into the bulk of (μ, ν, T) space? As noticed in Ref. [3], the same trick used originally to derive the chiral spiral, namely a chiral rotation with a linearly x-dependent phase, can be applied to the isospin case as well. This shows that the phase boundaries of the isoNJL model are independent of ν, just like the phase boundary of the NJL model is independent of μ. The full phase diagram can thus be generated by simply translating the GN phase diagram rigidly into the direction of the ν axis, see Fig. 2. The resulting mean field is the product of the GN mean field and the NJL chiral spiral phase factor,

$$S \mp iP_3 = S_{\mathrm{GN}}(\mu, T, x)e^{\pm 2i\nu x}. \tag{8}$$

The structure of a double helix emerges where up and down contributions have opposite handedness. This gives rise to three distinct phases of the massless isoNJL model: A chirally restored one (*I*), a double chiral spiral with constant radius (*II*), and a double chiral spiral with x-dependent radius, modulated by the shape of the GN kink crystal (*III*). One finds that this solution is self-consistent, in spite of the fact that $P_{1,2} = 0$ has been assumed from the outset. No better HF solution (with neutral and charged pion condensates) has been found so far, including the earlier variational calculations [8,9].

This is the status of the phase diagrams of models (1)–(3) in the chiral limit. The purpose of the present paper is to continue investigating the phase diagram of the massive isoNJL model. As already known from the one-flavor models, we cannot expect an analytical solution any more, but have to engage in numerical calculations as well. This complicates matters significantly, but the phase diagram is also expected to be richer than in the chiral limit.

The paper is organized as follows. In Sec. II we review what is known about the phase diagram of the massive isoNJL model to date. In Sec. III we outline a method recently proposed to find the exact tricritical point in the massive NJL model. In Sec. IV we adapt this method to the massive isoNJL model and present detailed results for the full phase diagram, including for the first time the tricritical curve in (μ, ν, T) space.

II. CONSTRUCTING THE PHASE DIAGRAM OF THE MASSIVE isoNJL MODEL

We now turn to the massive versions of models (1)–(3) by adding the Dirac mass term (4) to each Lagrangian. Here, the phase diagrams of the GN and NJL model are again known analytically (massive GN [10]) or at least numerically (massive NJL [11]). Recall that during renormalization, the two bare parameters m_b and G^2 are traded for the physical fermion mass in vacuum (m) and the so-called "confinement parameter" (γ) according to the gap equation

$$\frac{\pi}{2N_c G^2} = \gamma + \ln\frac{\Lambda}{m}, \qquad \gamma = \frac{\pi m_b}{2N_c G^2 m} = \frac{m_b}{m}\ln\frac{\Lambda}{m}. \tag{9}$$

Here, $\Lambda/2$ is the momentum cutoff, and Eq. (9) arises at the vacuum level like in the simplest GN model (for a pedagogical introduction, see Ref. [6]). This version belongs to the two-flavor isoNJL model (3). In the case of the one-flavor models (1), (2), replace G^2 by $g^2/2$. We use units such that $m = 1$ for any γ in the following. The Dirac HF equation for the massive isoNJL model is unchanged as compared to (5), but the self-consistency conditions (6) now read

$$\begin{aligned} S - m_b &= -G^2\langle\bar\psi\psi\rangle, \\ \vec{P} &= -G^2\langle\bar\psi i\gamma_5\vec\tau\psi\rangle. \end{aligned} \tag{10}$$

We assume once again that the charged components of $\vec{P}$ vanish. Then the reasoning used in the chiral limit goes through literally, yielding a Hamiltonian diagonal in isospin space and Eq. (5) for up and down quarks. Let us start again by looking at the special cases where one of the chemical potentials vanishes. The problem then reduces to the single-flavor GN ($\nu = 0$) and NJL ($\mu = 0$) phase diagrams, now for the massive models. Here, only two phases exist, a massive homogeneous one and an inhomogeneous one with spatially periodic order parameter, see Fig. 3. The massless phase is forbidden since chiral symmetry is explicitly broken by the bare mass. On the NJL side, the "horizontal" solid line is a perturbative second-order phase boundary determined via a stability analysis. The "vertical" dotted curve is a first-order phase boundary inferred from a numerical HF calculation. The homogeneous solution and a periodic inhomogeneous solution with finite amplitude coexist along this line. These two curves meet at a tricritical point indicated by a dot. Originally, this point had been found by pushing the numerical HF calculation towards the endpoint of the first-order line ("bottom up" approach [12]). More recently, a new method based on next-to-leading-order (NLO) perturbation theory has been devised to find the exact position of the tricritical point from the perturbative side ("top down" approach [13]), superseding the earlier numerical result. On the GN side, the horizontal part also belongs to a second-order phase transition accessible via a stability analysis. Upon crossing it, the system becomes unstable against the creation of a periodic structure of infinitesimal amplitude.

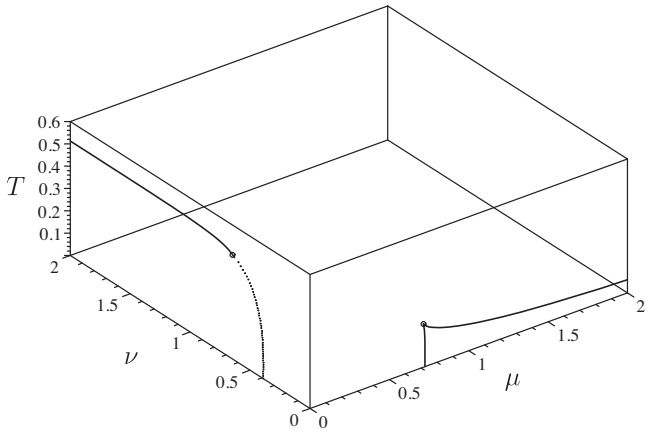

FIG. 3. Boundary phase diagram of the massive isoNJL model ($\gamma = 0.1$) if one of the chemical potentials vanishes. At $\nu = 0$, it is the same as the massive GN model. At $\mu = 0$, it is the same as the massive NJL model with chemical potential ν.

The vertical part is nonperturbative. Here, the system is unstable against formation of a single baryon. At the cusp, there is a tricritical point, and the wave number of the inhomogeneous phase vanishes. The massive GN results have been obtained in an analytical way [10]. Let us also mention that the base points of the phase boundaries at $T = 0$ are located at the masses of the most strongly bound baryons in both models. Their values are known from independent works, analytically in the GN model [14] and numerically in the NJL model [15].

Due to the different character of the phase diagrams on the boundaries $\nu = 0$ and $\mu = 0$, it is interesting to study how the massive isoNJL model will manage to interpolate between the two graphs if both chemical potentials are nonvanishing. Figure 3 immediately shows that the interpolating phase boundary sheet must depend nontrivially on all three coordinates, in contrast to the chiral limit of Fig. 2. An inspection of Fig. 3 suggests to split the problem into four distinct questions: How are the horizontal perturbative phase boundaries connected? What is the curve in the $T = 0$ plane, connecting the two base points and separating homogeneous from inhomogeneous phases at zero temperature? What is the shape of the phase boundary sheet connecting the two vertical nonperturbative curves? And, finally, what is the shape of the tricritical curve connecting the two tricritical points? The first three questions have already been answered [3,12]. We illustrate the solution in Secs. II A–II C, using as an example the case $\gamma = 0.1$. The last question is the main topic of the present work and will be covered in Secs. III and IV.

A. Perturbative sheet and stability analysis

If we set $P_1 = P_2 = 0$, then the grand canonical potential of the isoNJL model can be written as a sum over two NJL model expressions,

$$\Psi_{\mathrm{isoNJL}}(\mu,\nu,T,S,P_3) = \Psi_{\mathrm{NJL}}(\mu+\nu,T,S-iP_3) + \Psi_{\mathrm{NJL}}(\mu-\nu,T,S+iP_3). \quad (11)$$

This equation holds provided we use $G^2 = g^2/2$ and the same γ parameter on both sides. Solving the isoNJL model is therefore closely related to solving the NJL model. We start with the easiest part of the phase diagram, the perturbative second-order phase boundaries separating the homogeneous from the inhomogeneous phases. The stability analysis consists in the following steps: perturb the massive Dirac Hamiltonian by a harmonic potential of the form

$$V = \gamma^0 2S_1 \cos(2Qx) - i\gamma^1 2P_1 \sin(2Qx), \quad (12)$$

evaluate analytically the shift of the single particle energies in second-order perturbation theory, and expand the grand canonical potential to leading order in the correction. This still has to be minimized with respect to m, Q, S_1, P_1. At the phase boundary, m is the same as the fermion mass in the homogeneous phase. Due to (11), many formulas can be taken over from the NJL model. The minimizations amount to setting the Hessian determinant and its derivative with respect to Q equal to 0,

$$\det \mathcal{M} = 0, \qquad \partial_Q \det \mathcal{M} = 0, \quad (13)$$

with $\mathcal{M}$ the Hessian matrix

$$\mathcal{M} = \begin{pmatrix} \partial_{S_1}^2 \Psi & \partial_{S_1}\partial_{P_1}\Psi \\ \partial_{P_1}\partial_{S_1}\Psi & \partial_{P_1}^2 \Psi \end{pmatrix}. \quad (14)$$

In such a leading order (LO) stability analysis, not all of the parameters can be determined. Aside from the critical temperature as a function of μ, ν, one can extract the ratio $R = S_1/P_1$ and the wave number Q, but not the overall strength of the perturbation. R and Q characterize the unstable mode. They are not immediately relevant for the location of the phase boundary, but will play a role for finding the tricritical point.

Although technically quite simple, such a stability analysis gives already a fairly good impression of the full phase diagram. It is available for a number of γ values [3]. In the example at hand ($\gamma = 0.1$), the result is shown in Fig. 4, smoothly interpolating between GN and NJL perturbative critical curves. As expected from the boundary phase diagrams at $\mu = 0$ and $\nu = 0$, this calculation leaves open the details of the homogeneous "wound" around $\mu = 0$, $\nu = 0$. This will be the subject of the upcoming subsections and sections.

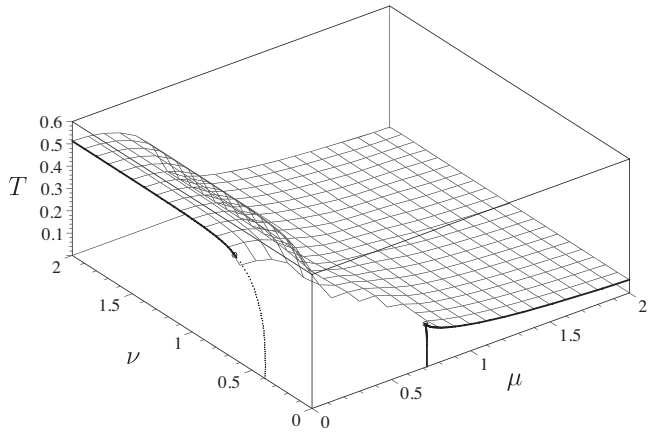

FIG. 4. Adding the perturbative second-order sheet to the phase diagram of Fig. 3. The surface is the result of a LO stability analysis [3] and interpolates between the horizontal perturbative second-order phase boundaries of GN and NJL model at $\nu = 0$ and $\mu = 0$, respectively.

B. Nonperturbative phase boundary in the $T = 0$ plane and baryon masses

The next step is to find the phase boundary at $T = 0$, connecting the base points of the GN and NJL phase diagrams. These latter are given by the masses of the most strongly bound baryons of the two models and are known analytically (M_{GN}) or numerically (M_{NJL}) in the massive models, as a function of γ. Since these base points are now also part of the isoNJL phase diagram at $T = 0$, the two-flavor isoNJL model must possess baryons with the same masses. As shown in Ref. [12], M_{GN} is the mass of the isoNJL baryon with maximal baryon number and zero isospin, consisting of N_c up quarks and N_c down quarks. M_{NJL} is the mass of the baryon with zero baryon number and maximal isospin made out of N_c up quarks and N_c down antiquarks. Many other multifermion bound states with different baryon number and isospin are expected to also play a role along the phase boundary in the $T = 0$ plane. This has been investigated in Ref. [12]. Somewhat surprisingly, apart from M_{GN} and M_{NJL}, only one other baryon mass enters into the construction of the phase boundary: the mass M_{up} of the baryon with half maximal baryon number and half maximal isospin, consisting solely of N_c up quarks. The result for the phase boundary is the first quadrant of an octagon with vertices at the points $(\mu,\nu) = (M_{\mathrm{GN}}, 2M_{\mathrm{up}} - M_{\mathrm{GN}})$ and $(2M_{\mathrm{up}} - M_{\mathrm{NJL}}, M_{\mathrm{NJL}})$, see Fig. 5. It can be made up by intersecting the three lines

$$\nu = M_{\mathrm{NJL}}, \qquad \mu = M_{\mathrm{GN}}, \qquad \mu + \nu = 2M_{\mathrm{up}}, \quad (15)$$

where $M_{\mathrm{NJL}} = 0.3853$, $M_{\mathrm{GN}} = 0.7240$, $M_{\mathrm{up}} = 0.4129$ at $\gamma = 0.1$. Actually, the octagon shape results from constructing the envelope of a whole family of straight lines and seems to be universal for all γ values. In order to construct this family and the envelope, the masses of all

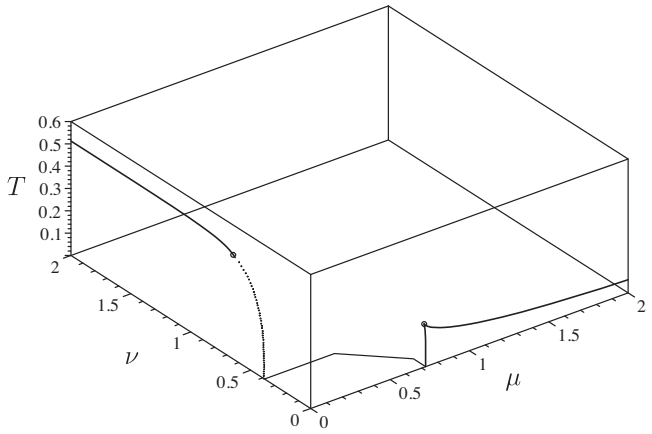

FIG. 5. Adding the nonperturbative phase boundary in the $T = 0$ plane to the phase diagram of Fig. 3. As shown in Ref. [12], it has the shape of the first quadrant of an octagon and is fully determined by three baryon masses of the isoNJL model, see main text.

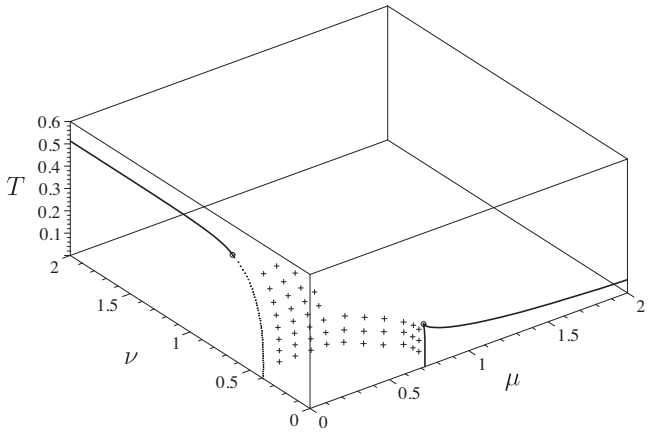

FIG. 6. Adding the first-order sheet at $T > 0$ (crosses) to the phase diagram of Fig. 3. It interpolates between the vertical nonperturbative phase boundaries of the GN ($\nu = 0$) and NJL ($\mu = 0$) models. From numerical HF calculation [12].

possible baryons had to be computed numerically in HF, even though only three masses are needed eventually.

C. First-order sheet at finite T and summary

The most tedious part of the calculation is the nonperturbative sheet interpolating between the vertical nonperturbative phase boundaries of GN and NJL models. It requires a full numerical HF calculation. One has to evaluate the grand canonical potential for the mean fields $S(x), P_3(x)$. These are assumed to be periodic with wave number q and parametrized in terms of their Fourier components S_ℓ, P_ℓ. For a given point (μ, ν, T), one has to minimize the effective potential with respect to all the S_ℓ, P_ℓ, and q. One chooses a trajectory across the anticipated phase boundary and compares the result with the homogeneous solution. If one finds two curves intersecting at a point along the trajectory, this point belongs to the first-order phase boundary sheet. The result for $\gamma = 0.1$ from Ref. [12] is shown in Fig. 6 (crosses). It interpolates between the nonperturbative curves on the boundary and also matches nicely onto the octagon shape of the $T = 0$ phase boundary. The technique used here is identical to the one developed previously for the massive NJL model, so that we do not go into further details. All points shown were clearly identified as first-order transitions.

Finally, we put all the ingredients discussed so far together in one plot, Fig. 7. This summarizes the state of the art of the massive isoNJL phase diagram at present, for the example of $\gamma = 0.1$. We find a consistent picture, supporting our assumption that $\vec{P}_\perp = 0$. All the different pieces based on independent calculations and a variety of techniques fit together very well, like the pieces of a a jigsaw puzzle. The most glaring deficit is probably the fact that we do not know yet how to interpolate between the tricritical points. Hence the line separating the first- and second-order sheets remains poorly defined. As mentioned in Ref. [12], numerical HF calculations in this region were not precise enough, a difficulty first encountered in the massive NJL model. Recently, a better method has been proposed, tailored to the tricritical points and, in principle, exact [13]. This will be reviewed and applied to the case at hand, the massive isoNJL model, in the next two sections.

III. PRECISE DETERMINATION OF THE TRICRITICAL CURVE

Recently, a novel method of locating the tricritical point has been devised and tested successfully in the massive NJL model [13]. The basic idea is to start from the stability analysis, but pushing perturbation theory to NLO (fourth

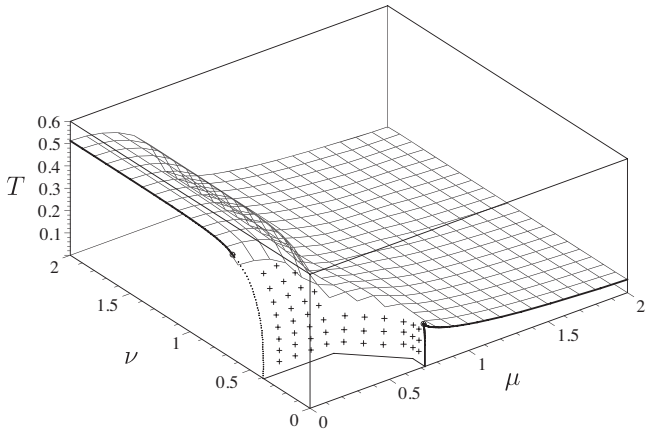

FIG. 7. Present status of the massive isoNJL phase diagram at $\gamma = 0.1$, constructed by putting together the ingredients shown in Figs. 3–6. A tricritical curve connecting the tricritical points of the GN and NJL models on the boundaries is still missing. From [12].

order in S_1, P_1). In the case of the single-flavor NJL model, the procedure may be summarized as follows:

(1) Find a point on the perturbative sheet close to where the tricritical point is expected via a LO stability analysis. Find the coordinates (μ, ν, T) together with the ratio $R = S_1/P_1$ and the wave number Q of the unstable mode.

(2) Do a fourth-order perturbative evaluation, first of the HF single particle energies and then of the thermodynamic potential, keeping R, Q fixed at the LO values. The remaining parameters are m, P_1.

(3) Choose 3 masses $m_0, m_0 \pm \Delta m$ with m_0 the mass of the homogeneous solution at point (μ, ν, T) on the perturbative sheet and $\Delta m \ll m_0$. Minimize the grand canonical potential for each mass value with respect to P_1. The resulting effective potential is a function of m only,

$$\tilde{\Psi}(m) = \min_{P_1} \Psi(m, P_1). \tag{16}$$

(4) The criterion for the tricritical point is the vanishing of the second derivative of the effective potential, $\partial_m^2 \tilde{\Psi}|_{m_0}$ or, in discretized form,

$$\frac{\tilde{\Psi}(m_0 + \Delta m) - 2\tilde{\Psi}(m_0) + \tilde{\Psi}(m_0 - \Delta m)}{\Delta m^2} = 0. \tag{17}$$

The main technical difficulty which had to be overcome is the fact that perturbation theory breaks down near the spectral gaps of a periodic potential. This becomes more serious in higher order perturbation theory where the usual LO "almost degenerate perturbation theory" cannot be applied any more. The way out is to go via an effective Hamiltonian in the space of strongly mixed states and diagonalize it exactly, using a formalism from many-body perturbation theory due to Lindgren [16]. The method has been shown to work very well for the massive NJL model and is supposedly exact, just like the LO stability analysis for the perturbative sheet.

When applying this method to the isoNJL model, all we have to do is use Eq. (11) and reduce the technicalities to those of the NJL model. One question which then arises is this: Can we be sure that the criterion developed for the massive NJL model also applies to the isoNJL model? The nature of the two tricritical points on the boundaries $\nu = 0$ (GN) and $\mu = 0$ (NJL) seems to be very different at first glance. In the NJL model, the two phase boundaries adjacent to the tricritical point meet tangentially under 0°, whereas the corresponding angle is 180° at the cusp of the GN model. On the other hand, since we have the representation (11) of the isoNJL model as a sum of two NJL models, it is plausible that the methods for finding the tricritical points in both models are closely related. As an additional check, we have applied the method of Ref. [13] to the GN model. Since $P_1 = 0$, there are minor changes in the stability analysis. The unstable mode is only characterized by Q; there is no ratio R. In the fourth-order perturbative calculation, one can use the machinery developed in Ref. [13] by simply setting $P_1 = 0$. We have evaluated the second derivative (17) for several μ values near the tricritical point. The result is shown in Fig. 8 for $\gamma = 0.3$. We have not quite succeeded in reaching the point where the second derivative vanishes. However, as the figure shows, we can come very close to it. A linear extrapolation from the two last points then yields the value $\mu = 0.799$, in excellent agreement with the known GN tricritical point at the same γ ($\mu = 0.7986$). The same kind of agreement was reached at other values of γ. Apparently, the tricritical point in the GN model lies right at the edge of the perturbative sheet, but this is not expected for any other point on the tricritical curve. Thus we are confident that the perturbative method of locating the tricritical point can also be trusted in the isoNJL model. The results will be presented in the following section.

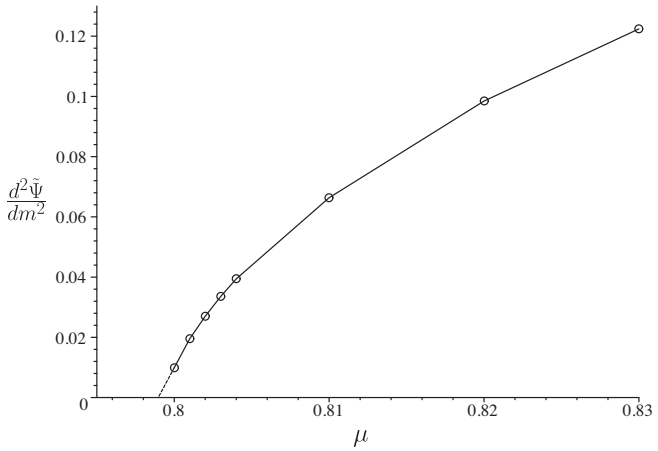

FIG. 8. Proof that the NLO stability analysis developed for the NJL model is also capable of locating the tricritical point of the massive GN model. The example $\gamma = 0.3$ is shown. The second derivative of the effective potential could be followed as a function of μ down to $\mu = 0.8$ (circles). Extrapolation to 0 yields the value $\mu = 0.799$, in excellent agreement with the known tricritical point.

IV. RESULTS AND DISCUSSION

We have computed the tricritical curve still missing in the phase diagram Fig. 7 for the massive isoNJL at $\gamma = 0.1$. The method has been sketched above and explained in more detail in Ref. [13], where it was applied to the massive NJL model. The main complication of the two-flavor model is the fact that we now have to determine a full curve of unknown shape and location, except for the endpoints. This means that we have to repeat the NLO perturbative calculation many times, each calculation being basically the same as for the one-flavor NJL model. Our result for $\gamma = 0.1$ is shown in Fig. 9. The tricritical curve

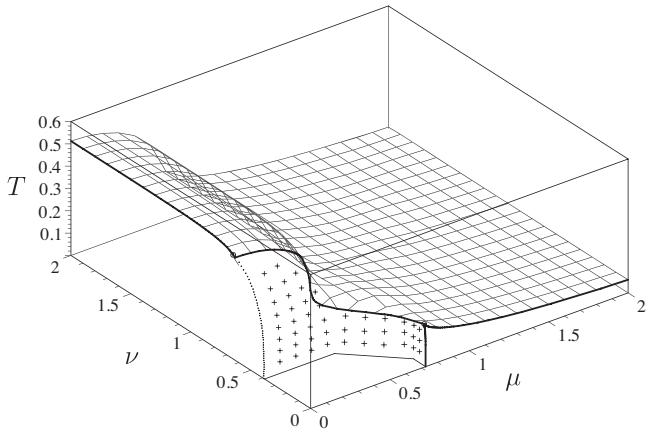

FIG. 9. Final phase diagram for the massive isoNJL model at $\gamma = 0.1$. The tricritical curve has been added to the previous phase diagram Fig. 7, now delimiting more clearly second-order and first-order sheets of the phase boundary between homogeneous and inhomogeneous phases.

thus obtained is fully compatible with the other building blocks of the phase diagram and enables us to delimit the inhomogeneous region of the phase diagram in a quantitative way.

In order to exhibit the shape of the tricritical curve in greater detail, we propose to look at its projection onto the $T = 0$ plane. The result is shown in Fig. 10 for $\gamma = 0.1$. We have marked the points which have actually been calculated by circles. The fat solid line is an interpolating curve and corresponds to the tricritical curve shown in the 3D Fig. 9. Due to the complicated shape of the tricritical curve, a fairly large number of points was needed. We have also included the $T = 0$ phase boundary into Fig. 10, the thin polygon.

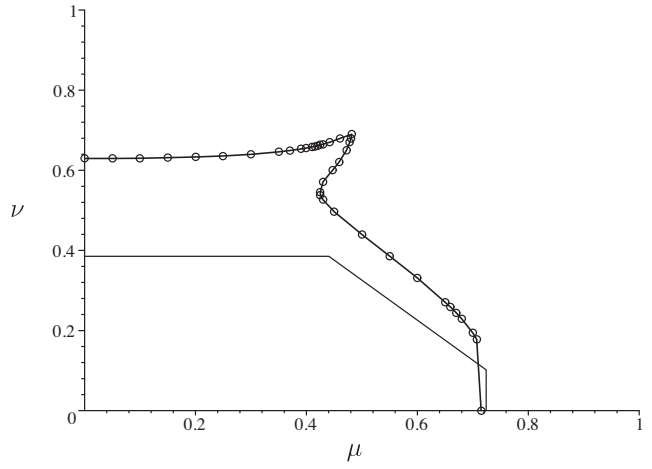

FIG. 10. Projection of tricritical curve onto the $T = 0$ plane for $\gamma = 0.1$. The circles are the points actually computed; the fat curve is just an interpolation which has been used for Fig. 9. The thin polygon is the phase boundary at $T = 0$ and $\gamma = 0.1$ discussed in Sec. II B. Relevant baryon masses: $M_{\mathrm{GN}} = 0.7240$, $M_{\mathrm{NJL}} = 0.3853$, $M_{\mathrm{up}} = 0.4129$.

The tricritical curve and the base curve are obviously correlated. At $T = 0$, we know that the instability along the three straight line segments is determined by three different baryons. Correspondingly, we shall refer to the three segments as GN (near $\nu = 0$), up (tilted), and NJL (near $\mu = 0$) parts. A similar division can be made for the first-order sheet and the tricritical line. The GN and NJL parts are still strongly influenced by the boundary phase diagrams. In these regions, the temperature drops to a common level. The up region seems to be the one with the simplest features. The projected tricritical curve follows the slope of the line $\mu + \nu = \mathrm{const}$, the first-order sheet is steep and essentially planar, and the temperature is slowly varying. This is perhaps the most interesting part since it has no correspondence in the one-flavor phase diagrams. As speculated in Ref. [13], it is quite likely that there are additional phase boundaries inside the crystal phase, starting from the vertices of the $T = 0$ octagon and going inside the crystal region. If this is true, then the question arises, what happens if we go up in temperature? If the internal phase boundary would persist all the way through the inhomogeneous phase, then there should be phase boundaries in addition to the tricritical curve discussed so far. We have searched for this with our method of finding tricritical points, but without success. This indicates that if such internal phase boundaries really exist at $T = 0$, then they disappear at some temperature below the perturbative sheet.

In Ref. [13], the nonperturbative sheet of the massive isoNJL phase diagram has been evaluated at three values of γ, 0.1, 0.2, and 0.3. Therefore, we have also repeated the calculation of the tricritical curve for $\gamma = 0.2$ and $\gamma = 0.3$ to see the evolution with increasing bare fermion mass. The 3D plots are shown in Figs. 11 and 13, along with the projections onto the $T = 0$ plane and the $T = 0$ phase boundaries in Figs. 12 and 14. Qualitatively, the three phase diagrams and tricritical curves at the three different γ values look very similar. As is particularly striking in the projections, the up part becomes more dominant with increasing γ and the simpler features of that part of the phase boundary

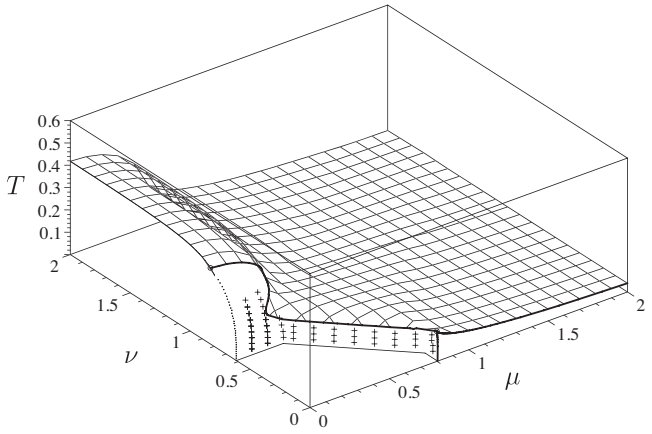

FIG. 11. Same as Fig. 9, but for $\gamma = 0.3$.

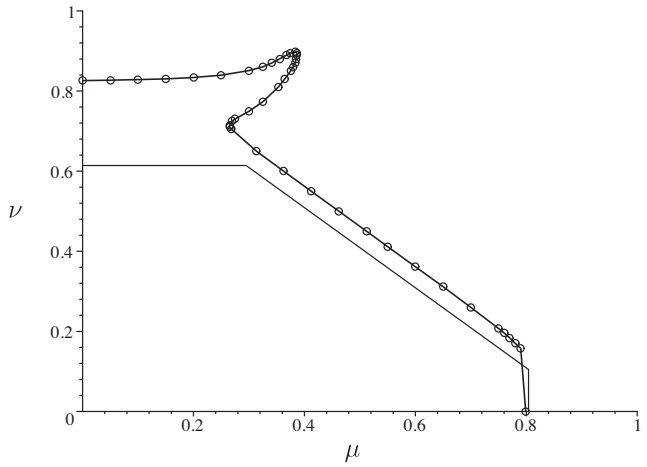

FIG. 12. Same as Fig. 10, but for $\gamma = 0.3$. Relevant baryon masses: $M_{\rm GN} = 0.8041$, $M_{\rm NJL} = 0.6142$, $M_{\rm up} = 0.4546$.

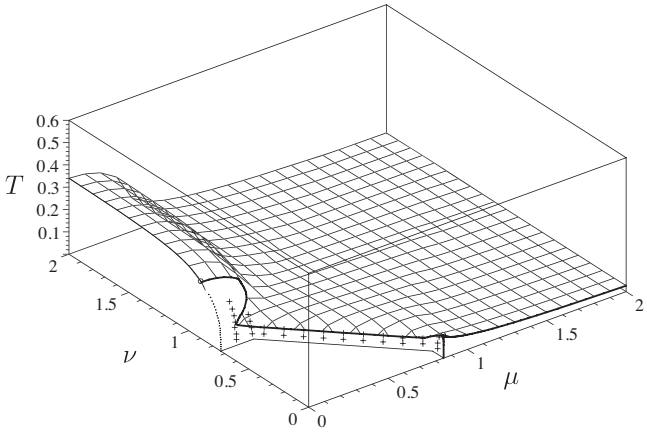

FIG. 13. Same as Fig. 9, but for $\gamma = 0.5$.

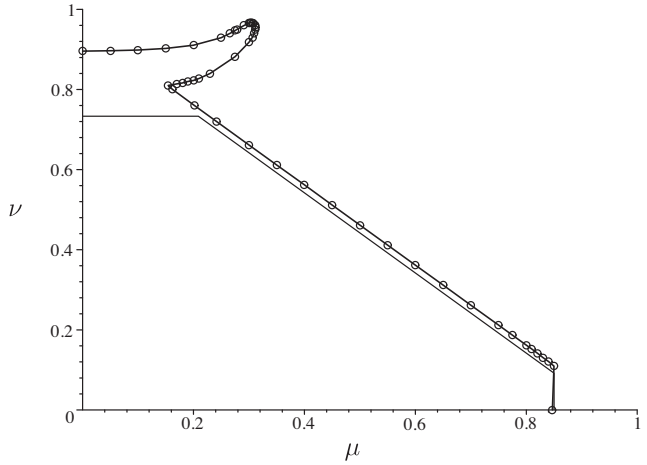

FIG. 14. Same as Fig. 12, but for $\gamma = 0.5$. Relevant baryon masses: $M_{\rm GN} = 0.8501$, $M_{\rm NJL} = 0.7334$, $M_{\rm up} = 0.4710$.

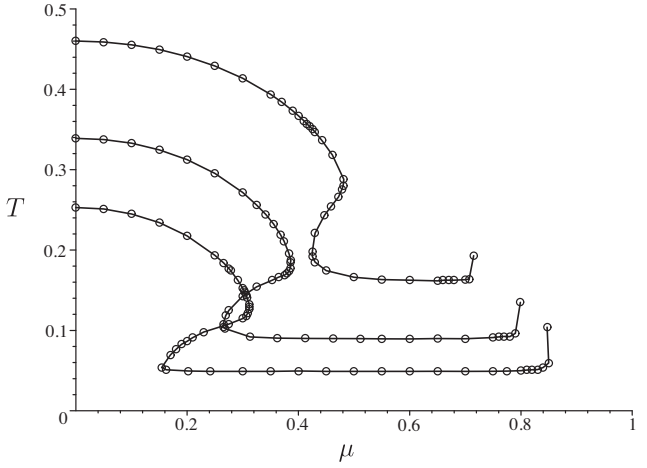

FIG. 15. Projection of tricritical curves onto the $\nu = 0$ plane. From top to bottom: $\gamma = 0.1$, 0.3, 0.5.

show up more clearly. Thus, at the highest γ, the $T = 0$ line and the projection of the tricritical curve are almost indistinguishable and account for a large part of the phase boundary, see Fig. 14. The strong variation of the projected tricritical curve near the largest ν values (the "nose") is a reflection of the part of the curve which rises steeply in temperature, as can be inferred from the 3D plot, Fig. 13.

As mentioned above, the up parts of the tricritical curves have essentially constant temperature and, at the same time, the lowest one along the whole tricritical curve. In order to exhibit this effect more clearly, we have also plotted projections of the three tricritical curves onto the (μ, T) and (ν, T) planes, see Figs. 15 and 16. Common to all bare masses is the observation that the temperature decreases in the GN section, stays constant through the up section, and increases more strongly in the NJL section. This reinforces the impression that the physics in the up section should be most easily accessible, perhaps by using some heavy quark approximation for large γ.

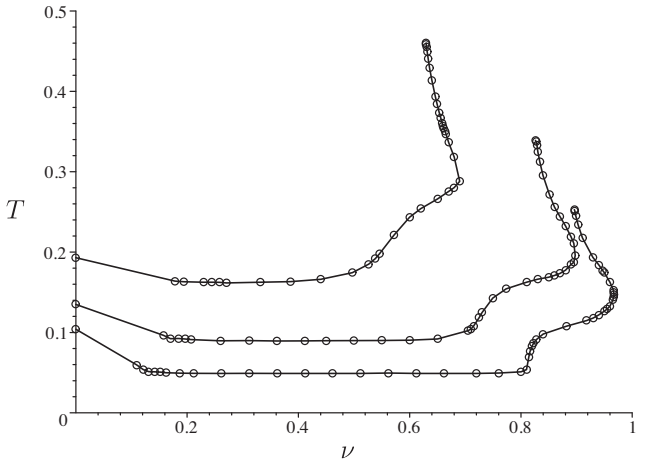

FIG. 16. Projection of tricritical curves onto the $\mu = 0$ plane. From top to bottom: $\gamma = 0.1$, 0.3, 0.5.

[1] D. J. Gross and A. Neveu, Phys. Rev. D **10**, 3235 (1974).
[2] Y. Nambu and G. Jona-Lasinio, Phys. Rev. **124**, 246 (1961).
[3] M. Thies, Phys. Rev. D **101**, 014010 (2020).
[4] A. Heinz, F. Giacosa, M. Wagner, and D. H. Rischke, Phys. Rev. D **93**, 014007 (2016).
[5] O. Schnetz, M. Thies, and K. Urlichs, Ann. Phys. (Amsterdam) **314**, 425 (2004).
[6] V. Schön and M. Thies, *At the Frontier of Particle Physics: Handbook of QCD, Boris Ioffe Festschrift*, edited by M. Shifman (World Scientific, Singapore, 2001), Vol. 3, Chap. 33, p. 1945.
[7] G. Basar, G. V. Dunne, and M. Thies, Phys. Rev. D **79**, 105012 (2009).
[8] T. G. Khunjua, K. G. Klimenko, R. N. Zhokhov, and V. C. Zhukovsky, Phys. Rev. D **95**, 105010 (2017).
[9] T. G. Khunjua, K. G. Klimenko, and R. N. Zhokhov, Phys. Rev. D **100**, 034009 (2019).
[10] O. Schnetz, M. Thies, and K. Urlichs, Ann. Phys. (Amsterdam) **321**, 2604 (2006).
[11] C. Boehmer, U. Fritsch, S. Kraus, and M. Thies, Phys. Rev. D **78**, 065043 (2008).
[12] M. Thies, Phys. Rev. D **101**, 074013 (2020).
[13] M. Thies, Phys. Rev. D **105**, 116003 (2022).
[14] M. Thies and K. Urlichs, Phys. Rev. D **71**, 105008 (2005).
[15] C. Boehmer, F. Karbstein, and M. Thies, Phys. Rev. D **77**, 125031 (2008).
[16] I. Lindgren, J. Phys. B **7**, 2441 (1974).